Effects of Filtering and Current-angle Adjustment on the Multi-Material Topology Optimization of a 3-phase Stator

Théodore Cherrière, S. Hlioui, Luc Laurent, François Louf, Hamid Ben Ahmed, Mohamed Gabsi

Effects of Filtering and Current-angle Adjustment on the Multi-Material Topology Optimization of a 3-phase Stator

Théodore Cherrière[*,a]
Sami Hlioui[b]
Luc Laurent[c,d]
François Louf[e]
Hamid Ben Ahmed[f]
Mohamed Gabsi[a]

[a] SATIE laboratory, ENS Paris-Saclay, CNRS, Université Paris-Saclay, 91190 Gif-sur-Yvette, France
[b] SATIE Laboratory, CY Cergy Paris University, CNRS, Paris-Saclay University, 95000 Cergy, France
[c] Laboratoire de Mécanique des Structures et des Systèmes Couplés, EA 3196, Conservatoire national des arts et métiers, F-75003 Paris, France
[d] HESAM University, Paris, France
[e] LMPS - Laboratoire de Mécanique Paris-Saclay, Université Paris-Saclay, CentraleSupélec, ENS Paris-Saclay, CNRS, 91190 Gif-sur-Yvette, France
[f] SATIE Laboratory, ENS Rennes, CNRS, 35170 Bruz, France
[*] Corresponding author
theodore.cherriere@ens-paris-saclay.fr

Abstract

This paper investigates the multi-material topology optimization of the 3-phase stator of an electrical machine. The density-based optimization framework uses a gradient descent on the physical properties of the candidate materials (magnetic polarization and current density). The results indicate that a smoothing procedure is necessary to avoid non-manufacturable designs and promotes a broader exploration of solutions. They also highlight a current angle shifting due to the presence of permanent magnets from the beginning of the optimization. The current angle is therefore added to the optimization variables to address this issue. An efficient optimization procedure that couples both techniques is proposed to improve the performance of the algorithm. The following hybrid method returns symmetrical results that perform better than the asymmetrical structures obtained with the other techniques applied independently, indicating that the asymmetry represents a local optimum.

Keywords: Boundary conditions – Filtering – Multi-Material – Topology Optimization – Permanent magnet machines – Stator

- Open Archive HAL with file: hal-04213621
- Doi: 10.1109/TMAG.2023.3317700

Contents

1 Introduction

TOPOLOGY optimization is an automatic conception tool that aims to find an optimized distribution of materials to minimize an objective function f. First introduced in mechanical engineering [1], it was then extended to electrical actuators by Dyck and Lowther [2]. Density-based approaches are the most popular among several methods [3] and have been widely applied in electrical engineering. Most of the applications in electrical machines deal with the rotors [4], [5]; the stators are included much less frequently [6]. Density methods can handle multiple materials by solving the following optimization problem

$$\text{find} \quad \boldsymbol{\rho}_{\text{opt}} = \arg\min_{\boldsymbol{\rho}\in\mathcal{D}^N} f(\boldsymbol{\rho}), \tag{1}$$

where $\boldsymbol{\rho}$ is the vector of optimization variables, N the number of mesh elements to fill with a material, and $\mathcal{D}$ is an interpolation domain, such as $[0,1]$ for iron/air case. Air is represented by $\rho = 0$, whereas $\rho = 1$ represents steel, and $0 < \rho < 1$ describes fictive intermediate materials. This relaxation enables using gradient-based algorithms that efficiently handle many optimization variables ($N > 10^3$). In Multi-Material Topology Optimization (MMTO), $\mathcal{D}$ is a polytope associating its vertices to different materials. The interpolation can be built using shape functions [7], similar to the generalized finite element interpolant [8]. An example for $n_m = 8$ materials listed in Table 1 is shown in Figure 1.

Table 1: Candidate materials numbering

Indices i	1	2	3	4	5	6	7	8
Materials	A^+	C^-	B^+	A^-	C^+	B^-	***Iron***	*Air*

The optimization problem (1) is generally ill-posed, which leads to numerical artifacts and mesh dependency. In particular, the optimized designs may contain thin microstructures that are non-manufacturable. Convolutive density filtering [9] inspired by image processing is a standard procedure to address this issue by ensuring a minimal length scale to the design. While artifacts are not always apparent [10], a strong regularization process is essential to obtain meaningful structures in complex MMTO problems [5]. Since anti-periodic boundary conditions are commonly used to simulate only one pole of an electrical machine, special attention should be paid to boundary management during the filtering process.

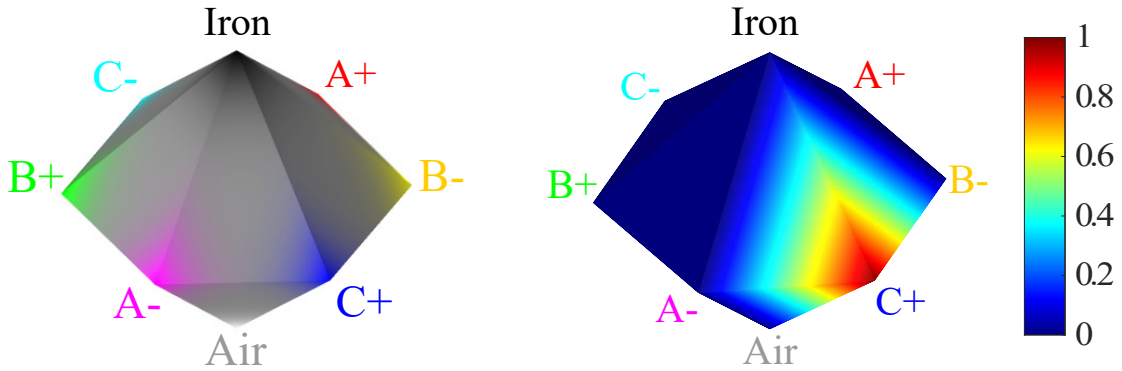

(a) Interpolation domain $\mathcal{D}$ (b) Values of a shape function associated to C^+

Figure 1: Interpolation domain which supports a set of shape functions.

This work studies various MMTO methodologies to optimize the 3-phase stator of a Permanent Magnet Synchronous Machine (PMSM). It is organized as follows: Sec. 2 describes the optimization process and details the mathematical tools. Numerical experiments in Sec. 3 show that this MMTO problem is subject to geometrical artifacts and current angle misadjustment. These results indicate that a new hybrid optimization procedure is needed. Finally, Sec. 4 compares and discusses the methodologies proposed in the previous section.

2 Optimization framework

In this paper, we optimize the stator of a 3-phase permanent magnet synchronous machine to maximize its average torque $\langle T \rangle$ computed by Arkkio's method [11] with a density approach so that $f = -\langle T \rangle$. The magnetostatic problem is discretized with the finite element method [12] into a matrix $\mathbf{K}$ and a right-hand side $\boldsymbol{s}$:

$$\mathbf{K}\boldsymbol{a} = \boldsymbol{s}(\tilde{\boldsymbol{m}}(\boldsymbol{\rho}, \boldsymbol{a}), \tilde{j}(\boldsymbol{\rho})), \tag{2}$$

that is solved on 60 rotor positions to get the magnetic state $\boldsymbol{a}$ from the interpolated material properties $\tilde{j}$ and $\tilde{\boldsymbol{m}}$. Then, a Projected Gradient Descent (PGD) using the adjoint variable method [13] is performed. The $n_m = 8$ candidate materials are listed in Table 1 and placed on the vertices of a polytope $\mathcal{D}$ as in Fig. 1a, such that the optimization problem reads as (1).

2.1 Material interpolations

The current densities of the i material from Table 1 reads

$$j_i = \begin{cases} J\cos(\theta_e - (i-1)\pi/3 + \psi) & \text{if } i \leq 6, \\ 0 & \text{else,} \end{cases} \tag{3}$$

with θ_e the electric angle synchronized with the rotation of the rotor, J the current density amplitude set to $10\,\mathrm{A/mm^2}$ and ψ the current angle. The iron BH curve is the same as in [12].

Magnetic polarizations $\boldsymbol{m}$ and current densities j are interpolated with shape functions [8]. The shape function ω associated with C^+ is plotted in Fig. 1b as an example. The interpolations of the materials' properties read [13]

$$\tilde{\boldsymbol{m}}(\boldsymbol{\rho}, \boldsymbol{b}) = \sum_{i=1}^{n_m} P_m(\omega_i(\boldsymbol{\rho}))\boldsymbol{m}_i(\boldsymbol{b}), \tag{4a}$$

$$\tilde{j}(\boldsymbol{\rho}) = \sum_{i=1}^{n_m} P_j(\omega_i(\boldsymbol{\rho}))j_i, \tag{4b}$$

where P_m, P_j are the penalization functions associated with $\boldsymbol{m}$ and j, respectively. P_m and P_j are RAMP functions [14], with the coefficients $q_m = 3$ and $q_j = 1$, respectively.

2.2 Multi-material filtering

Multi-material regularization is based on a convolutive density filter. The material properties of each mesh element $\mathcal{T}$ are averaged on a circular kernel $\mathcal{K}$ centered on the barycenter of $\mathcal{T}$ with radius R. Let us define Ω and $\overline{\Omega}$ as the simulation domain and its complementary. The anti-periodicity boundary conditions are taken into account by wrapping: when a part of $\mathcal{K}$ is beyond the simulation domain Ω, then the corresponding material properties are deduced from its opposite side to ensure the filtering continuity through the border, as shown in Fig. 2.

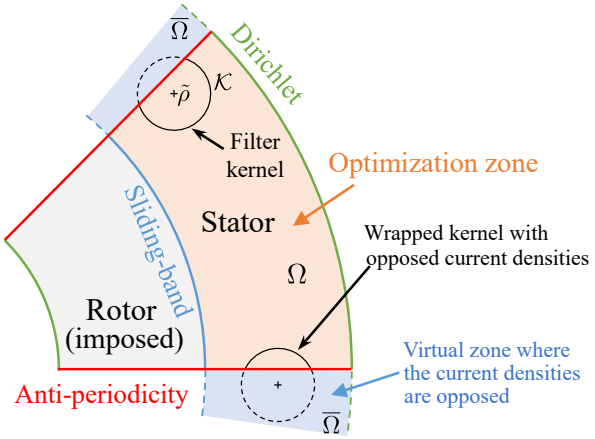

Figure 2: Simulation zone with the wrapped kernel and boundary conditions.

Special care should be paid to the current densities that are opposed due to anti-periodicity: A^+ becomes A^-, B^+ becomes B^-, C^+ becomes C^- and vice versa, defining a material permutation Π. Thus, the transformed density $\overline{\boldsymbol{\rho}}$ located in $\overline{\Omega}$ that matches this material permutation reads

$$\overline{\boldsymbol{\rho}} = \sum_{i=1}^{n_m} \omega_i(\boldsymbol{\rho}) \boldsymbol{v}_{\Pi(i)}, \tag{5}$$

where $\boldsymbol{v}_i$ is the coordinate of the i-vertex of the polytope $\mathcal{D}$. This equality (5) holds assuming the candidate materials set contains the negative counterpart of each electric conductor and if the set of basis functions verifies the following linear precision property

$$\forall \boldsymbol{\rho} \in \mathcal{D}, \quad \boldsymbol{\rho} = \sum_{i=1}^{n_m} \omega_i(\boldsymbol{\rho}) \boldsymbol{v}_i, \tag{6}$$

as in the case of the shape functions used in this work [8]. If these conditions are satisfied, the filtered density $\tilde{\rho}$ then reads

$$\tilde{\boldsymbol{\rho}} = \frac{1}{|\mathcal{K}|} \left(\int_{\mathcal{K} \cap \Omega} \boldsymbol{\rho} + \int_{\mathcal{K} \cap \overline{\Omega}} \overline{\boldsymbol{\rho}} \right). \tag{7}$$

3 Numerical experiments

The torque of the reference design adapted from a BMWi3 pole [15] and shown in Fig. 4a is first computed for each current angle ψ and reaches its maximum at $\psi_{\text{opt}} = 288°$. Thus, ψ is set to ψ_{opt}

during optimization. Initially, all $\boldsymbol{\rho}$ terms are in the barycenter of $\mathcal{D}$, corresponding to the design plotted in Fig. 4b. Figure 3 shows the global optimization algorithm.

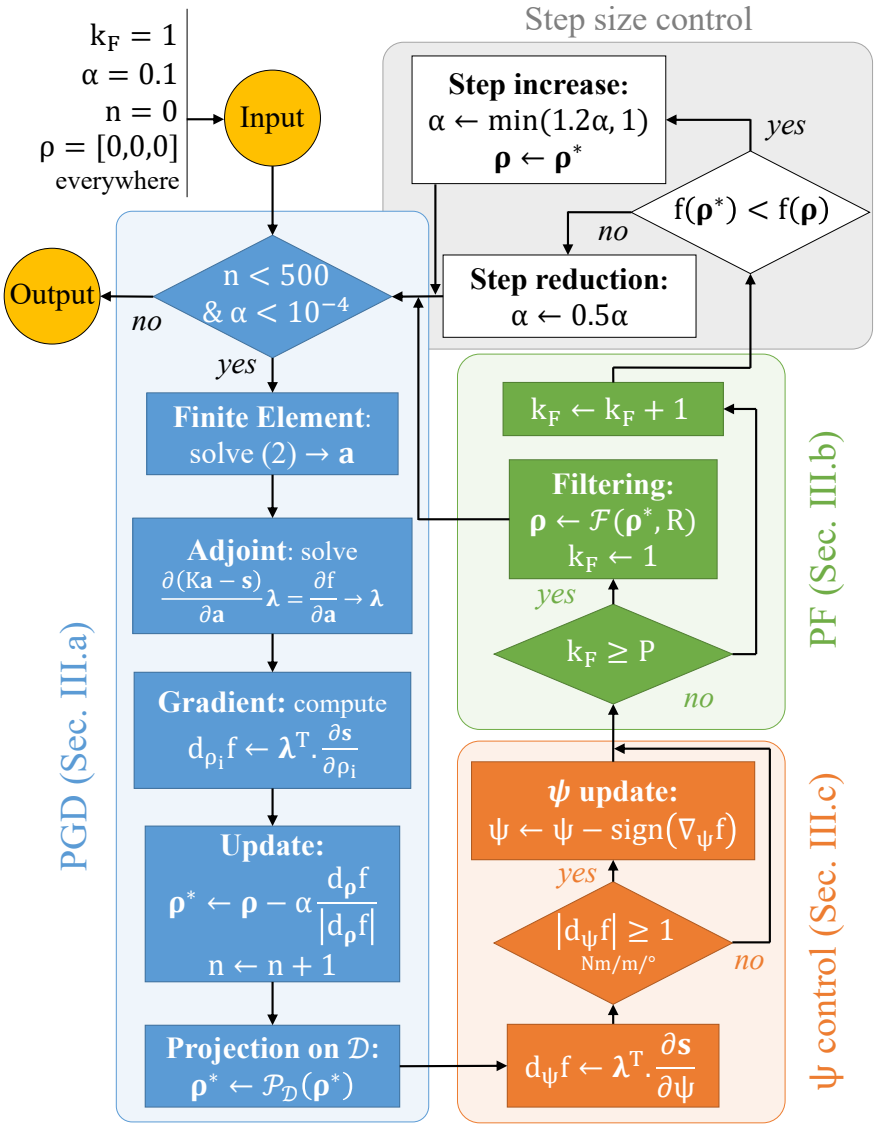

Figure 3: Flowchart of the optimization algorithm.

3.1 Naïve projected gradient descent

First, only the PGD and the step control blocks of the algorithm given in Fig. 3 are enabled. We note that the result adopts a different topology than the reference to maximize its torque at the expense of torque ripple, which is not considered in the optimization and is doubled. The torque evolution during the optimization and the obtained design are shown in Fig. 5. The final average torque is lower than the reference and contains non-manufacturable isolated materials that should vanish. Density filtering is a simple solution to remove them.

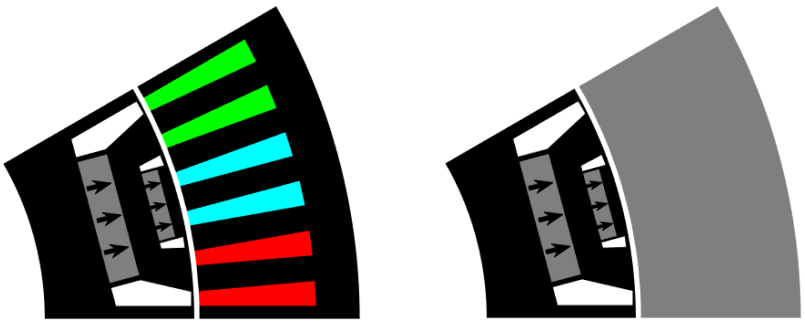

(a) Reference adapted from [15] (b) Initial design

Figure 4: Reference design (2173 Nm/m) and initial situation.

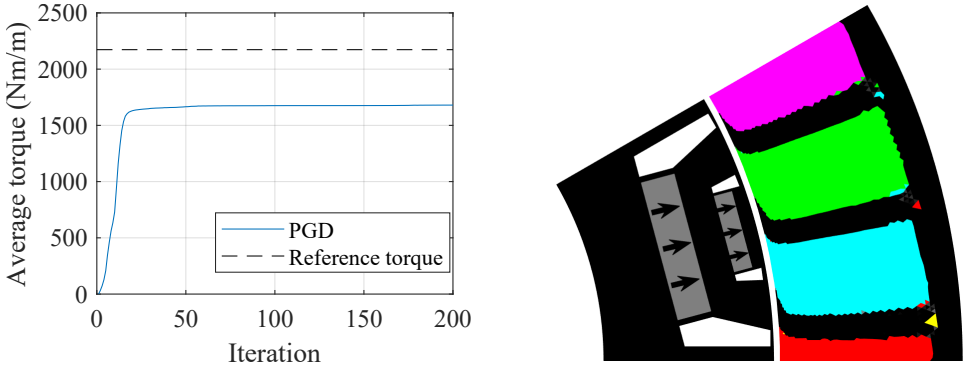

(a) $\langle T \rangle$ during optimization (b) Final design

Figure 5: Optimization results with a simple PGD.

3.2 Periodic filtering

Next, the optimization is performed with the Periodic Filtering (PF) block shown in Fig. 3, which depends on the period P and the kernel radius R. PF was introduced because filtering at each iteration ($P = 1$) prevents obtaining sharp interfaces and leads to bad performance. The results of a parametric study on the effect of the values of P and R shown in Fig. 6a exhibit minimal admissible values: $R > 0.5\,\text{mm}$ should be bigger than the size of a mesh element, and $P > 1$ to avoid disturbing the optimization process at each iteration.

Filtering removes the isolated materials as expected but also significantly changes the optimized design. Specifically, Fig. 8 shows that the structure is progressively rotated in the trigonometric direction, while the torque envelope shown in Fig. 7 increases slowly ; the oscillations are due to the PF and not to an instability of the algorithm. This result suggests that the current angle ψ is misadjusted, which will be further analyzed in Sec. 4.

3.3 Adjustment of the current angle

A new approach to deal with such a misadjustment involves treating ψ as an optimization variable. Since the nature of this new variable (electric angle) is different from the other design variables, ψ is adjusted by a thresholded gradient descent as shown in Fig. 3. The adjoint variable method calculates the corresponding sensitivity $\mathrm{d}_\psi \langle T \rangle$. In the results given in Fig. 9, the PF is disabled. It was checked that the ψ control converges to the maximum torque per ampere angle, which leads quickly to a higher torque than the reference, as shown in Fig. 9a. However, because geometrical artifacts remain in Fig. 9b, both techniques – PF and ψ adjustment – should be coupled.

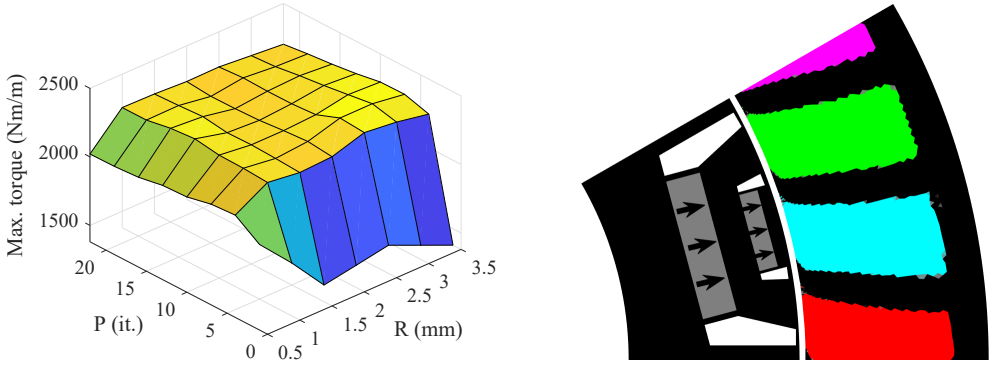

(a) Effect of filtering parameters (b) Best design with filtering

Figure 6: Optimization results with filtering procedure.

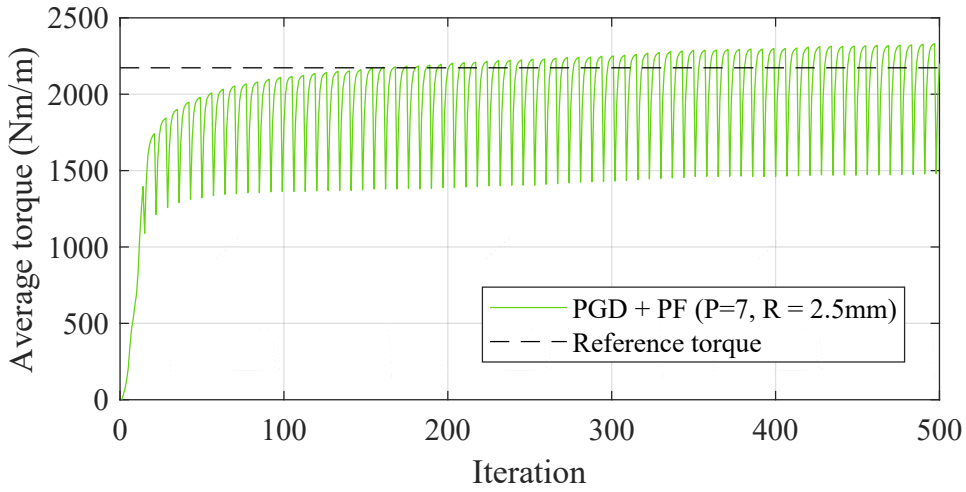

Figure 7: Typical evolution of the torque with PF.

3.4 Hybrid method

Lastly, PF (Sec. 3.2) and ψ control (Sec. 3.3) are hybridized, and the full algorithm of Fig. 3 is used. Since PF considerably disturbs the torque and the current angle, we choose $P = 20$ and $R = 2.5\,\text{mm}$. The results are shown in Fig. 10: the optimized structure reaches a higher torque than the other methods, as reported in Fig. 10a. The resulting stator slots are symmetric and shown in Fig. 10b, whereas the previous structures shown in Fig. 5b, 6b and 9b are asymmetric.

4 Discussion

The previous study shows that the hybrid method quickly returns higher torques than the other methods. Table 2 gives a comparison of the methods. The ψ misadjustment can explain the variation of algorithms performances due to the unbalanced contribution of the magnet torque T_m compared with the reluctance torque T_r, each of these components being associated with a different optimal angle ψ [16]

$$\langle T \rangle = \underbrace{\langle [I_s(\boldsymbol{\rho})]^T \frac{\mathrm{d}L_{sr}(\boldsymbol{\rho})}{\mathrm{d}\theta} [I_r] \rangle}_{T_m} + \underbrace{\frac{1}{2} \langle [I_s(\boldsymbol{\rho})]^T \frac{\mathrm{d}L_{ss}(\boldsymbol{\rho})}{\mathrm{d}\theta} [I_s(\boldsymbol{\rho})] \rangle}_{T_r}, \tag{8}$$

with $[I_s]$ the stator currents, $[I_r]$ the rotor currents equivalent to the permanent magnets, L_{sr} the mutual

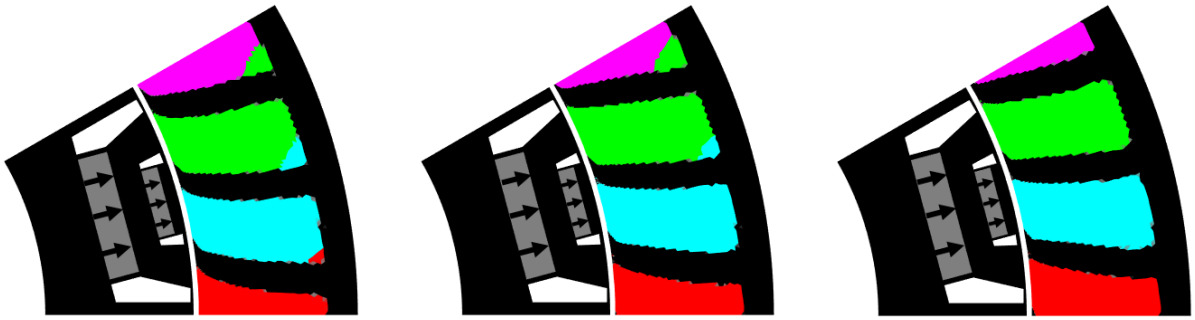

(a) It. n°104 (b) It. n°252 (c) It. n°399

Figure 8: Snapshots of the design during the optimization with PF.

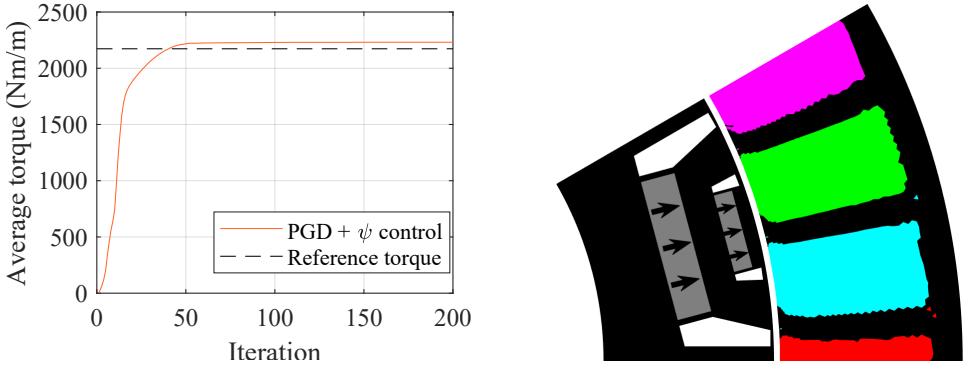

(a) $\langle T \rangle$ during optimization (b) Final design

Figure 9: Optimization results with a PGD and a ψ control.

matrix inductance between $[I_r]$ and $[I_s]$, and L_{ss} the self-inductance of $[I_s]$. Since $[I_s]$ is initially 0, $\mathrm{d}_{\boldsymbol{\rho}} T_r = 0$, while $[I_r]$ is fixed by the permanent magnet so that $\mathrm{d}_{\boldsymbol{\rho}} T_m \neq 0$. As a result, only the magnet torque is maximized at the beginning of the optimization. Later during the optimization, when the importance of T_r increases, ψ should be adjusted, which is not allowed in Sec. 3.1 and 3.2. The other degree of freedom is the mechanical rotation, which is limited because of the material interpolations' penalizations that break the convexity of the problem [17]. Therefore, only the zone near the airgap, where the sensitivity is highest, may move to compensate for ψ misadjustment, leading to an asymmetrical local optimum. PF in Sec. 3.2 enables more mechanical rotation by repeatedly blurring the interfaces so they can move slightly. Because this is a slow process, its combination with current angle adjustment is efficient for getting performing results as in Sec. 3.4.

Table 2: Comparison of the different optimization algorithms

Performance	**Ref.**	**PGD**	**PGD + PF**	**PGD + ψ control**	**Hybrid**
$\langle T \rangle_{\max}$ (Nm/m)	2173	1680	2331	2231	2484
Iteration at $0.99\langle T \rangle_{\max}$	-	49	420	47	50

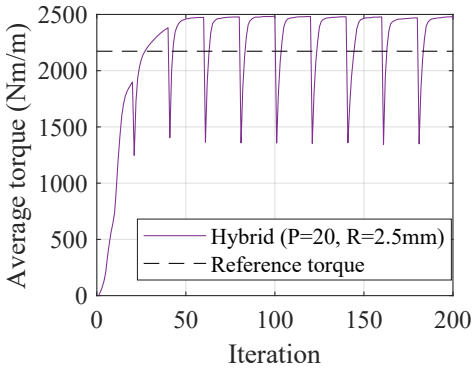

(a) Evolution of $\langle T \rangle$ and ψ

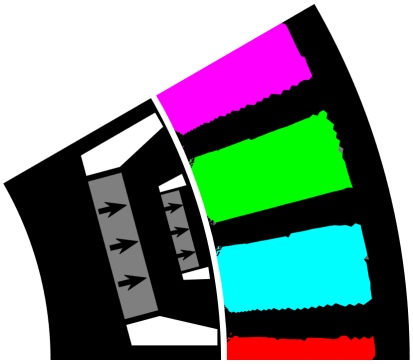

(b) Final design

Figure 10: Results obtained with filtering and ψ adjustment.

5 Conclusion

This paper investigates MMTO methods to design 3-phase PMSM stators, showing that a usual gradient descent leads to non-manufacturable local optima. A multi-material density filtering consistent with the antiperiodic boundary conditions smooths the structure and promotes a broader exploration of solutions. A current angle adjustment accelerates the optimization, and the combination of both techniques quickly converges to a symmetric design with a higher torque than the asymmetric structures obtained by other methods applied independently.

Future research will consider other objective functions (such as torque ripple), more physics (mechanical stress), and both stator and rotor simultaneously.

References

[1] M. P. Bendsøe and N. Kikuchi, "Generating optimal topologies in structural design using a homogenization method," *Computer methods in applied mechanics and engineering*, vol. 71, no. 2, pp. 197–224, 1988 (cit. on p. 2).

[2] D. N. Dyck and D. A. Lowther, "Automated design of magnetic devices by optimizing material distribution," *IEEE Transactions on Magnetics*, vol. 32, no. 3 PART 2, pp. 1188–1192, 1996. DOI: 10.1109/20.497456 (cit. on p. 2).

[3] F. Lucchini, R. Torchio, V. Cirimele, *et al.*, "Topology Optimization for Electromagnetics: A Survey," *IEEE Access*, vol. 10, no. August, pp. 98 593–98 611, 2022. DOI: 10.1109/access.2022.3206368 (cit. on p. 2).

[4] J. Lee, J. H. Seo, and N. Kikuchi, "Topology optimization of switched reluctance motors for the desired torque profile," *Structural and Multidisciplinary Optimization*, vol. 42, no. 5, pp. 783–796, 2010. DOI: 10.1007/s00158-010-0547-1 (cit. on p. 2).

[5] C. Lee and I. Gwun, "Multi - material topology optimization for the PMSMs under the consideration of the MTPA control," *Structural and Multidisciplinary Optimization*, pp. 1–11, 2022 (cit. on p. 2).

[6] T. Labbé and B. Dehez, "Convexity-Oriented Mapping Method for the Topology Optimization of Electromagnetic Devices Composed of Iron and Coils," *IEEE Transactions on Magnetics*, vol. 46, no. 5, pp. 1177–1185, 2010. DOI: 10.1109/CEFC.2010.5481713 (cit. on p. 2).

[7] M. Bruyneel, "SFP—a new parameterization based on shape functions for optimal material selection: Application to conventional composite plies," *Structural and Multidisciplinary Optimization*, vol. 43, no. 1, pp. 17–27, 2011. DOI: 10.1007/s00158-010-0548-0 (cit. on p. 2).

[8] E. L. Wachspress, *A Finite Element Rational Basis* (Mathematics in Science and Engineering). Academic Press, Inc., 1975, vol. 114. DOI: 10.1016/s0076-5392(09)60113-2 (cit. on pp. 2–4).

[9] O. Sigmund and J. Petersson, "Numerical instabilities in topology optimization: A survey on procedures dealing with checkerboards, mesh-dependencies and local minima," *Structural Optimization*, vol. 16, no. 1, pp. 68–75, 1998. DOI: 10.1007/BF01214002 (cit. on p. 2).

[10] J. S. Choi and J. Yoo, "Simultaneous structural topology optimization of electromagnetic sources and ferromagnetic materials," *Computer Methods in Applied Mechanics and Engineering*, vol. 198, no. 27-29, pp. 2111–2121, 2009. DOI: 10.1016/j.cma.2009.02.015 (cit. on p. 2).

[11] A. Arkkio, "Analysis of Induction Motors Based on the Numerical Solution of the Magnetic Field and Circuit Equations.," Ph.D. dissertation, Helsinki University of Technology, 1987 (cit. on p. 3).

[12] T. Cherrière, T. Vancorsellis, S. Hlioui, *et al.*, "A multimaterial topology optimization considering the pm nonlinearity," *IEEE Transactions on Magnetics*, vol. 59, no. 5, pp. 1–9, 2023. DOI: 10.1109/TMAG.2023.3256003 (cit. on p. 3).

[13] T. Cherrière, L. Laurent, S. Hlioui, *et al.*, "Multi-material topology optimization using Wachspress interpolations for designing a 3-phase electrical machine stator," *Structural and Multidisciplinary Optimization*, vol. 65, no. 352, 2022. DOI: 10.1007/s00158-022-03460-1 (cit. on p. 3).

[14] M. Stolpe and K. Svanberg, "An alternative interpolation scheme for minimum compliance topology optimization," *Structural and Multidisciplinary Optimization*, vol. 22, no. 2, pp. 116–124, 2001. DOI: 10.1007/s001580100129 (cit. on p. 4).

[15] D. Staton and J. Goss, "Open Source Electric Motor Models for Commercial EV & Hybrid Traction Motors," in *CWIEME*, Berlin, 2017 (cit. on pp. 4, 6).

[16] S. Seely, *Electromechanical energy conversion*. McGraw-Hill, 1962 (cit. on p. 7).

[17] M. Abdelhamid and A. Czekanski, "Revisiting non-convexity in topology optimization of compliance minimization problems," *Engineering Computations (Swansea, Wales)*, vol. 39, no. 3, pp. 893–915, 2022. DOI: 10.1108/EC-01-2021-0052 (cit. on p. 8).